IJRCS

International Journal of Robotics and Control Systems
Vol. 5, No. 3, 2025, pp. 1998-2015
ISSN 2775-2658
http://pubs2.ascee.org/index.php/ijrcs

ASCEE

Real-Time Experimental Study of Speed Control for PMSM Drive System on OPAL-RT Simulator Using Radial Basis Function Neural Network

Xuan Hung Hoang [a,1], Thanh Hai Tran [b,2], Phan Minh Than [a,3], Thanh Quyen Ngo [a,4,*], Van Sy Nguyen [c,5], Tong Tan Hoa Le [a,6]

[a] Faculty of Electrical Engineering Technology, Industrial University of Ho Chi Minh City, Vietnam
[b] Office of Planning and Investment, Industrial University of Ho Chi Minh City, Vietnam
[c] Faculty of Automotive Engineering Technology, Industrial University of Ho Chi Minh City, Vietnam
[1] 23740731.hung@student.iuh.edu.vn; [2] tranthanhhai@iuh.edu.vn; [3] phanminhthan@iuh.edu.vn;
[4] ngothanhquyen@iuh.edu.vn; [5] nguyenvansy@iuh.edu.vn; [6] letongtanhoa@iuh.edu.vn
* Corresponding Author

ARTICLE INFO

Article history
Received July 03, 2025
Revised September 08, 2025
Accepted October 04, 2025

Keywords
PMSM;
Adaptive Control;
RBFNN;
Real-Time;
OPAL-RT

ABSTRACT

This paper addresses the problem of improving speed control accuracy and disturbance rejection capability for Permanent Magnet Synchronous Motors (PMSMs), which are widely used in industrial applications requiring high-performance drives. Conventional controllers such as PID often exhibit limited performance under nonlinear and time-varying conditions. The sliding mode control combined with a Radial Basis Function Neural Network (RBFNN) is proposed to enhance robustness and adaptability to overcome these limitations. The main contribution of this study is the integration of an adaptive RBFNN to estimate and compensate for unknown disturbances in real time, ensuring precise and stable motor operation. The theoretical stability of the system is guaranteed based on Lyapunov's theory. The proposed method is implemented in a MATLAB/Simulink environment and tested on the OPAL-RT OP5707XG real-time hardware platform. The control system includes a speed loop using the RBFNN and a current loop for field-oriented control. The motor is subjected to varying speed commands in three stages to evaluate performance under dynamic conditions. Simulation results show that the RBFNN controller significantly improves speed tracking accuracy, reduces overshoot, and adapts better to sudden changes compared to conventional PID control. Real-time experimental results further confirm the effectiveness of the controller, despite the presence of noise and hardware delays. Current control performance also demonstrates better torque production and phase symmetry under dynamic loading with the RBFNN. A comparative analysis between simulation and experimental data highlights the practical applicability of the proposed approach.

1. Introduction

The demand for electric vehicles (EVs) is increasing to meet the requirements of sustainable development and environmental impact reduction. Carbon dioxide (CO_2) and nitrogen oxides (NO_x) emissions from fossil fuel vehicles not only negatively affect the environment but also cause many serious problems for human health. Compared with traditional motors in industrial applications, motors used in electric vehicles need to be able to flexibly adjust their speed to adapt to diverse operating conditions such as starting, stopping, accelerating, braking, and decelerating quickly and accurately. Among current motor technologies, permanent magnet synchronous motors (PMSMs) stand out with superior features such as high torque at low speeds, high power density, superior efficiency, low vibration and noise, and high reliability [1]. An effective EV drive system needs to ensure precise torque management to improve dynamic performance, safety, longevity, durability, and optimize the cost-performance ratio for users [2]. Meanwhile, traditional direct current (DC) motors exhibit many limitations, such as low efficiency, large weight, and poor reliability due to the existence of commutators and brushes. Although simple in design and suitable for low-speed applications, DC motors require high maintenance costs and have difficulty in precise control at low speeds [3]. Switched Reluctance Motor (SRM) is another notable option with a simple structure, high starting torque, good performance, and high reliability. However, the disadvantages of SRM are high noise and high torque ripple [4]. Meanwhile, induction motors (IMs) are widely used in EVs due to their high reliability, low noise, easy maintenance, and stable operation at high speeds, but require more complex control. Brushless DC motors (BLDCs) and PMSMs have similar structures; the main difference lies in the stator current waveform: BLDCs use trapezoidal waves while PMSMs use sine waves. As a result, PMSMs provide higher efficiency, greater power density, and lower torque ripple than other types of motors, making them the optimal choice for high-performance applications in EVs [5]-[7].

In most PMSM motor control applications, two common global control strategies are implemented: Direct Torque Control (DTC) and Field Oriented Control (FOC). DTC has a simpler control structure, which is implemented based on two discrete on/off hysteresis controllers to regulate the stator torque and flux. However, the main drawback of DTC is that it causes significant torque and current fluctuations, which negatively affect the overall performance of the PMSM drive system [8], [9]. In contrast, FOC is implemented as a series of hierarchical control structures, in which the outer control loop (open loop – OL) performs speed control and sets the q-axis current setpoint, while the d-axis current setpoint is usually maintained at zero to optimize torque. The inner control loop (closed loop – IL) precisely regulates the d–q current through the corresponding voltage control, in order to achieve linear control characteristics similar to those in conventional DC systems. Current and speed controllers in FOC often use proportional–integral (PI) controllers due to their simplicity and good tunability under nominal operating conditions. However, PI controllers are often limited in performance in nonlinear situations, primarily when the motor operates far from the design operating point. The main reasons come from changes in system parameters (such as reactance, time constant) and the impact of load torque disturbances [10], [11]. These significant challenges require effective handling to ensure accurate and stable control of the PMSM drive system. In studies [12], the authors proposed applying genetic algorithms to optimize the initial parameters of the FOPID controller. Although it brings certain efficiency in the initialization stage, this method shows limitations when deployed in a volatile environment, because the genetic algorithm only stops at determining the initial optimal parameter set without performing online correction during operation. Therefore, when the system is subjected to uncertain factors, it becomes difficult to maintain the desired stability and accuracy.

Due to the nonlinear nature and complex dynamic characteristics, the application of traditional linear control techniques to achieve optimal control performance for permanent magnet synchronous motors (PMSMs) is challenging. The main difficulties include inherent nonlinearity, high sensitivity to noise, and torque variation, which significantly affect the performance and accuracy of the control system. In response to this situation, many nonlinear control strategies have been developed to

improve the controllability of PMSMs under variable and uncertain working conditions. Nonlinear control methods include: Model Predictive Control (MPC) [13], Fuzzy Logic Control [14], Active Disturbance Rejection Control (ADRC) [15], [16], and Data-Driven Event-Triggered Adaptive Dynamic Programming Control [17], [18]. These methods are often used in cases where the mathematical model of the system is incomplete or inaccurate. In studies [19], [20], the parameter optimization problem of fuzzy controllers has been mentioned to improve control accuracy. However, a standard limitation of this method is that it requires the designer to deeply understand the system's characteristics and behavior to build a compatible and efficient controller. Moreover, during operation, the appearance of uncertain parameters that are difficult to predict in advance makes the design of a fixed controller less suitable. Therefore, developing controllers that can learn and adapt from errors is extremely necessary.

Many advanced control methods have been studied to overcome the above limitations, including adaptive control [21], [22], robust control [23], sliding mode control (SMC) [24], [25], de-noising control [26], as well as disturbance observation and estimation techniques [27], [28]. Among them, SMC – developed from the theory of variable structure control systems (VCS)-is evaluated to be outstanding due to its ability to tolerate parameter uncertainty, high noise immunity, and fast response time [29]-[35]. However, SMC still has some limitations in practical applications, mainly due to "chattering" – high-frequency oscillations that cause hardware wear and affect the system's stability. In addition, this method also requires an accurate mathematical model with complete information about physical parameters, making the implementation complicated [36], [37]. Many solutions have been proposed to reduce chattering, such as redesigning the sliding surface, replacing the sign function with a saturation function, or combining it with other soft control techniques [38]-[41]. Recently, fractional-order sliding mode control (SMC) has also received attention to improve performance and expand the design space by adding more degrees of freedom in the control structure [42]-[44]. Thanks to its simplicity in implementation, high anti-interference ability, and suitability for harsh operating environments, SMC is still considered one of the preferred solutions for PMSM control systems requiring high precision and robustness [45]-[51].

In order to simultaneously exploit the advantages of SMC and overcome the above limitations, this study integrates adaptive control technology into SMC to ensure both response speed and sustainability, as well as the ability to self-adjust parameters. In addition, modern control methods based on artificial neural networks (ANNs) have also received significant attention in recent years, thanks to their ability to approximate arbitrary nonlinear functions and high flexibility in system modeling [52]-[55]. A prominent approach is the disturbance-aware control strategy using the Radial Basis Function Neural Network (RBFNN) [54]. Due to its global learning properties and high adaptability, RBFNN is particularly suitable for handling nonlinear, unmodeled uncertainties and external disturbances in control systems such as electric drives and robot control. Furthermore, controllers combining RBFNN and online learning algorithms have shown great potential in improving control performance through the ability to update parameters in real time, ensuring convergence and fast response in changing environments [54]-[62]. These characteristics make RBFNN a prominent research trend in intelligent control strategies, especially in the context of increasingly complex, nonlinear and noise-sensitive systems.

1. The SMC ensures robustness, fast response, and system stability under parameter uncertainties and external disturbances. Béides, the RBFNN is designed to estimate and compensate for the total unknown disturbance in real time.
2. The RBFNN is designed to estimate the total unknown nonlinear disturbance, including external load torque and uncertainties existing in the system. In addition, RBFNN also contributes effectively to reducing the chattering phenomenon on the sliding surface.
3. The experiments are carried out in two environments: simulation on Simulink and Real-time on the OPAL-RT platform, to verify the feasibility of the proposed theory.

The rest of the paper is organized as follows. The mathematical model of the permanent magnet synchronous motor (PMSM) is presented in Section 2. Section 3 introduces the proposed controller in detail. Experiments to verify the effectiveness of the control scheme are carried out in Section 4. Finally, Section 5 provides the conclusions of the study.

2. Mathematical Model of PMSM Drive Systems

The model of the PMSM can be represented in the (d–q) coordinate system through the Park transformation, with the stator voltage equations on the d–axis and q–axis in the rotor reference frame as follows [63]-[64]:

$$\begin{cases} u_d = R_s i_d + L_d \dfrac{di_d}{dt} - \omega_e \lambda_q \\ u_q = R_s i_q + L_q \dfrac{di_q}{dt} + \omega_e \lambda_d \end{cases} \tag{1}$$

where $\lambda_q = L_q i_q$, $\lambda_d = L_d i_d + \varphi_f$; i_d and i_q are the d–q axis currents, u_d and u_q are the d–q axis voltages, R_s is the stator resistance, $L_q = L_d = L$ is the stator inductor, φ_f is the rotor flux linkage and ω_e is the electric angular speed. The equation describing the PMSM drive system motor according to the rotor is defined as follows [65]:

$$\begin{cases} \dfrac{di_d}{dt} = -\dfrac{R_s}{L} i_d + n_p \omega_m i_q + \dfrac{u_d}{L} \\ \dfrac{di_q}{dt} = -n_p \omega_m i_d - \dfrac{R_s}{L} i_q - \dfrac{n_p \varphi_f}{L} \omega_m + \dfrac{u_q}{L} \\ \dfrac{d\omega_m}{dt} = \dfrac{K_t}{J} i_q - \dfrac{B}{J} \omega_m - \dfrac{T_L}{J} \end{cases} \tag{2}$$

where $\omega_m = \frac{\omega_e}{n_p}$ is the rotor angular speed, n_p is the pole pairs, J is the rotor moment of inertia, B is the viscousfriction coefficient, T_L is the load torque. $K_t = 1.5 n_p \varphi_f$ is the torque constant. The mathematical model describing the dynamics of PMSM is formulated as:

$$J\dot{\omega}_m = T_e - B\omega_m - T_L \tag{3}$$

where $T_e = \frac{3}{2} n_p i_q \left[i_d \left(L_d - L_q \right) + \varphi_f \right] = \frac{3}{2} n_p \varphi_f i_q = K_t i_q$ is the electromagnetic torque. However, variations in the operating environment can cause deviations in parameters such as rotational inertia, rotor flux, and viscous friction coefficient, so the dynamic equation is adjusted to reflect these uncertainties as follows:

$$J_0 \dot{\omega}_m + \Delta J \dot{\omega}_m = \left(K_{t0} i_q + \Delta K_t i_q \right) - \left(B_0 \omega_m + \Delta B \omega_m \right) - T_L \tag{4}$$

where B_0, K_{t0}, and J_0 denote the nominal values of the viscous friction coefficient, torque constant, and moment of inertia, respectively. The terms $\Delta B, \Delta K_t$, and ΔJ represent the corresponding deviations from these nominal values, accounting for possible uncertainties or variations in the system's physical properties. Considering the discrepancies between actual and nominal parameters, the dynamic equation (4) can be simplified as follows:

$$\dot{\omega}_m = -\frac{B_0}{J_0} \omega_m + \frac{K_{t0}}{J_0} i_q - d \tag{5}$$

where $d = \frac{\left(\Delta J \dot{\omega}_m - \Delta K_t i_q + \Delta B \omega_m + T_L \right)}{J_0}$ represents the combined effect of parameter mismatch and load moment, which is considered as the sum of all disturbances existing around the system. However, in practice, these disturbance and uncertainty components are often not known accurately. Therefore,

this study proposes to use the RBFNN controller to estimate and compensate for the uncertainty components existing around the system to improve the accuracy and stability of the control system.

3. Controllers Design

Improving the control accuracy and performance of the system during operation is achieved by designing an RBFNN controller that acts as a nonlinear compensator to estimate and suppress the total disturbances affecting the PMSM system. The sliding surface is presented in [66] as follows:

$$s = e + c_1 \int_0^t e \, d\tau \tag{6}$$

where $e = \omega_m^{ref} - \omega_m$ is the speed error, ω_m^{ref} is the reference speed and $c_1 \geq 1$ is the integral gain. The derivative of Eq. (6) with respect to s is:

$$\dot{s} = -c_2 s - \mu sign(s) \tag{7}$$

where $c_2 \geq 1$ is identified as the amplification factor, and μ is a positive constant that adjusts the gain of the sliding mode control. The result of derivative both sides of Eq. (6) is:

$$\dot{s} = \dot{e} + c_1 e = \dot{\omega}_m^{ref} - \frac{K_{t0}}{J_0} i_q + \frac{B_0}{J_0} \omega_m + d + c_1 e \tag{8}$$

By defining d as the total disturbance and substituting Eq. (6) into Eq. (7), the resulting ideal control can be designed as follows:

$$i_q^{ref} = \frac{J_0}{K_{t0}} \left[\dot{\omega}_m^{ref} + \frac{B_0}{J_0} \omega_m + c_1 e + c_2 s + d + \mu sign(s) \right] \tag{9}$$

where i_q^{ref} is the $q - axic$ reference current.

Proof. The Lyapunov function is defined as follows:

$$V = s^2 \tag{10}$$

Derivative of Eq. (10):

$$\begin{aligned}
\dot{V} &= \frac{1}{2} s \dot{s} \\
\dot{V} &= \frac{1}{2} s (\dot{e} + c_1 e) \\
\dot{V} &= \frac{1}{2} s \left(\dot{\omega}_m^{ref} - \frac{K_{t0}}{J_0} i_q + \frac{B_0}{J_0} \omega_m + d + c_1 e \right) \\
\dot{V} &= \frac{1}{2} s \left[\dot{\omega}_m^{ref} - \frac{K_{t0}}{J_0} \frac{J_0}{K_{t0}} \left(\dot{\omega}_m^{ref} + \frac{B_0}{J_0} \omega_m + c_1 e + c_2 s + \mu sign(s) \right) + \frac{B_0}{J_0} \omega_m + d + c_1 e \right] \\
\dot{V} &= \frac{1}{2} s \left[\dot{\omega}_m^{ref} - \dot{\omega}_m^{ref} - \frac{B_0}{J_0} \omega_m - c_1 e - c_2 s - \mu sign(s) + \frac{B_0}{J_0} \omega_m + d + c_1 e \right] \\
\dot{V} &= \frac{1}{2} s [-c_2 s - \mu sign(s) + d]
\end{aligned} \tag{11}$$

Assuming $\mu \geq d$, Eq. (11) can be rewritten as follows:

$$\dot{V} = -\frac{1}{2} c_2 s^2 - \frac{1}{2} s \mu |s| + d \leq -\frac{1}{2} c_2 s^2 - \frac{1}{2} \mu s^2 \leq 0 \tag{12}$$

Remark. In Eq. (12), the amplification factor μ must be greater than the total disturbance d to guarantee system stability. Nonetheless, due to the nonlinear nature and uncertainty of d, selecting an

appropriate μ becomes challenging. A small μ may lead to system instability, whereas an excessively large μ may induce chattering phenomena. it is essential to estimate and compensate for the disturbance d, thereby allowing the use of a smaller μ that still maintains system stability and effectively mitigates chattering. Therefore, an adaptive RBFNN is designed in this subsection to estimate and compensate for the total online perturbation, allowing the use of a smaller gain factor μ while still ensuring system stability and reducing chattering.

The structure of the RBFNN is illustrated in Fig. 1. The RBF network consists of an input layer $\underline{x} = [x_1, x_2, \dots, x_n]^T$, a hidden layer $H(\underline{x}) = [h_1, h_2, \dots, h_m]^T$, a weight vector $W = [w_1, w_2, \dots, w_m]^T$, and an output layer y. In this study, the RBFNN is employed to approximate the unknown total disturbance d. Consequently, the input of the RBFNN selected as $x = [e, e_{i,q}]^T$, where $e_{i,q} = i_q^{ref} - i_q$ represents the $q - axit$ current tracking error. In order to balance the trade-off between approximation accuracy and computational complexity, the number of neurons j in the hidden layer is set to 5. Each neuron uses a Gaussian activation function, with a center vector $\boldsymbol{c}_j = [c_{1j}, c_{2j}]^T$ and widths b_j of the Gaussian function.

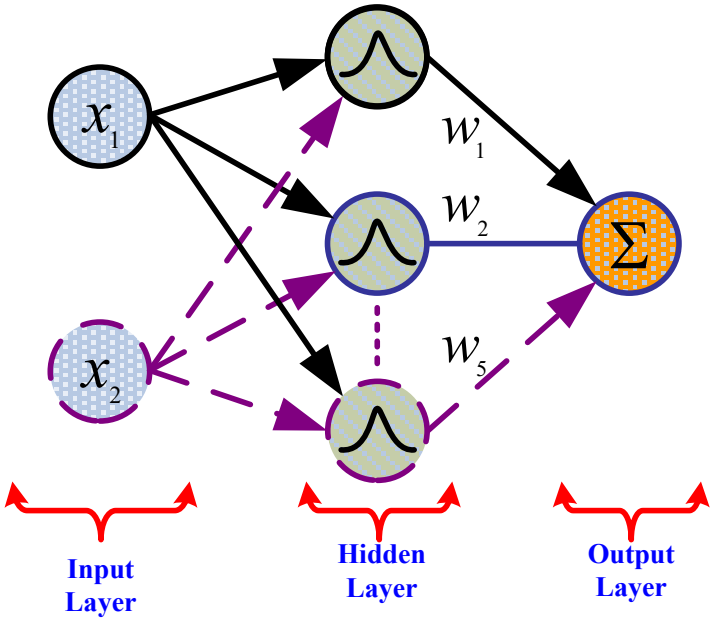

Fig. 1. Structure of radial basis function neural network

$$h_j = exp\left(-\frac{\|\underline{x} - \boldsymbol{c}_j\|^2}{2b_j^2}\right), j = 1,2,\dots,5 \tag{13}$$

The RBF neural network is used to approximate the total disturbance d, where d can be represented as follows:

$$d = W^{*T} H(\underline{x}) + \varepsilon \tag{14}$$

where ε is the approximate error, $W^{*T} = [w_1^*, w_2^*, \dots, w_5^*]$ is the ideal weight matrix. An online adaptive method is proposed to adjust the weight matrix W, aiming at achieving the ideal weight matrix W^*. Then, the output of the real-time neural network can be represented as follows:

$$\hat{d} = \hat{W}^T H(\underline{x}) \tag{15}$$

where $\hat{d}$ is an approximation of the total disturbance d, and $\hat{W}^T = [\hat{w}_1, \hat{w}_2, \dots, \hat{w}_5]$ is the adaptive weight matrix. The weight adaptation law $\dot{\hat{W}}^T = [\dot{\hat{w}}_1, \dot{\hat{w}}_2, \dots, \dot{\hat{w}}_5]$ is expressed as follows:

$$\dot{\hat{W}} = \eta s H(\underline{x}) \tag{16}$$

where $\eta > 0$ is gain factor, and s is the sliding surface Eq. (6). When the approximate value of the total disturbance $\hat{d}$ is inserted into Eq. (9), the control expression is obtained as follows:

$$i_q^{ref} = \frac{J_0}{K_{t0}}\left[\dot{\omega}_m^{ref} + \frac{B_0}{J_0}\omega_m + c_1 e + c_2 s + \hat{d} + \mu sign(s)\right] \tag{17}$$

Proof. The Lyapunov function is defined as follows:

$$\mathscr{L} = \frac{1}{2}s^2 + \frac{1}{2\eta}\tilde{W}^T\tilde{W} \tag{18}$$

where $\tilde{W} = W^* - \hat{W}$. The derivative of Eq. (18) yields the following result:

$$\dot{\mathscr{L}} = s\dot{s} + \frac{1}{\eta}\tilde{W}^T\dot{\tilde{W}} = s\left[\dot{\omega}_m^{ref} - \frac{K_{t0}}{J_0}i_q + \frac{B_0}{J_0}\omega_m + d + c_1 e\right] - \frac{1}{\eta}\tilde{W}^T\dot{\tilde{W}} \tag{19}$$

When applying control law Eq. (17) to Eq. (19), the expression obtained is as follows:

$$\begin{aligned}
&\dot{\mathscr{L}} = s\dot{s} + \frac{1}{\eta}\tilde{W}^T\dot{\tilde{W}} = s\left[\dot{\omega}_m^{ref} - \frac{K_{t0}}{J_0}i_q + \frac{B_0}{J_0}\omega_m + d + c_1 e\right] - \frac{1}{\eta}\tilde{W}^T\dot{\tilde{W}} \\
&\dot{\mathscr{L}} = s\left[\dot{\omega}_m^{ref} - \frac{K_{t0}}{J_0}\frac{J_0}{K_{t0}}\left(\dot{\omega}_m^{ref} + \frac{B_0}{J_0}\omega_m + c_1 e + c_2 s + \hat{d} + \mu sign(s)\right) + \frac{B_0}{J_0}\omega_m + d + c_1 e\right] - \frac{1}{\eta}\tilde{W}^T\dot{\tilde{W}} \\
&\dot{\mathscr{L}} = s\left[-c_2 s - \hat{d} - \mu sign(s) + d\right] - \frac{1}{\eta}\tilde{W}^T\dot{\tilde{W}}
\end{aligned} \tag{20}$$

Substituting the expressions in Eq. (14) and Eq. (15) into Eq. (20), the resulting expression is as follows:

$$\begin{aligned}
&\dot{\mathscr{L}} = s\left[-c_2 s - \hat{W}^T H(\underline{x}) - \mu sign(s) + W^{*T} H(\underline{x}) + \varepsilon\right] - \frac{1}{\eta}\tilde{W}^T\dot{\tilde{W}} \\
&\dot{\mathscr{L}} = s\left[-c_2 s - \mu sign(s) + \tilde{W}^T H(\underline{x}) + \varepsilon\right] - \frac{1}{\eta}\tilde{W}^T\dot{\tilde{W}} \\
&\dot{\mathscr{L}} = \tilde{W}^T\left[sH(\underline{x}) - \frac{1}{\eta}\dot{\tilde{W}}\right] - s\left[-c_2 s - \mu sign(s) + \varepsilon\right]
\end{aligned} \tag{21}$$

Finally, applying the weight adaptation law Eq. (16) to Eq. (21) leads to the following expression:

$$\begin{aligned}
&\dot{\mathscr{L}} = \tilde{W}^T[sH(\underline{x}) - sH(\underline{x})] + s[-c_2 s - \mu sign(s) + \varepsilon] \\
&\dot{\mathscr{L}} = s[-c_2 s - \mu sign(s) + \varepsilon] \le -c_2 s^2 \le 0
\end{aligned} \tag{22}$$

From Eq. (22), it can be observed that $-c_2 s^2 \le 0$. Therefore, the system achieves global asymptotic stability, with $s \to 0$ and $e \to 0$ as $t \to \infty$.

Fig. 2 illustrates a PMSM drive system based on rotor FOC, which consists of a speed control loop and two current control loops. Setting the d-axis reference current i_d^* to zero allows for achieving the optimal speed-to-current ratio and ensuring decoupling between current and speed control. PI controllers are implemented in the two current loops to suppress the *d*-*q*-axis current error and maintain system stability. The proposed control method is applied to the speed control loop in the PMSM drive system in this study.

4. Simulation and Real-Time Implementation Results

In this section, the experiments are conducted in two stages: simulation and real-time control on the OPAL-RT 5707 system. The aim is to evaluate the efficiency and reliability of the proposed

controller under different operating conditions. The parameters of the PMSM model used in the experiments are presented in Table 1, corresponding to the parameters described in Section 2.

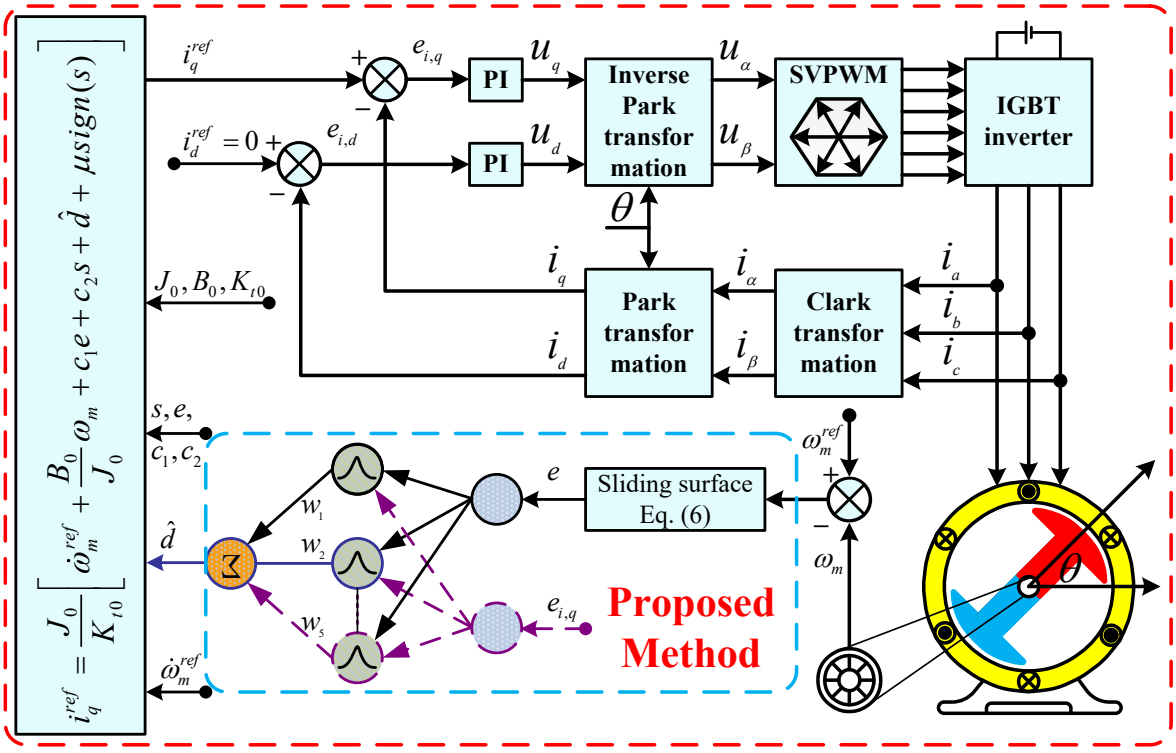

Fig. 2. An illustration of the control block diagram corresponding to the proposed method for PMSM

Table 1. PMSM parameters used in the experiment

Parameter	Value
Moment of inertia (B)	$3.5 \times 10^{-4} kg \cdot m^2$
Viscous damping coefficient (B)	$7.21 \times 10^{-5} N \cdot m \cdot s/rad$
Stator resistance (R)	1Ω
Stator inductor (L)	$6.25 \times 10^{-3} H$
Permanent magnet flux (φ_f)	$0.32 Wb$
Number of pole-pairs (n_p)	4

The parameters of the radial basis function neural network (RBFNN) are determined based on the synthesis of practical experience and previous research results of the authors in this field, to ensure suitability with the characteristics of the control object. RBFNN parameters used in the experiment shown in Table 2.

4.1. Simulation Results

The controlled object is a permanent magnet synchronous motor (PMSM) to evaluate the speed tracking ability of the system when applying the designed controller. The reference speed signal is set up in three stages: from 0 to 4 seconds, the speed increases from 0 to about 500 rpm and remains stable; from 4 to 7 seconds, the speed is increased rapidly to about 1250 rpm and maintained; from 7 to 10 seconds, the speed decreases to about 750 rpm. The model is built in the MATLAB/Simulink environment, including both the control block and the PMSM motor model. The controller used in the simulation is a previously designed RBFNN controller to ensure the ability to track the reference speed quickly, accurately, and stably. The actual speed signal of the motor in the simulation environment is recorded and compared with the reference signal to evaluate the control error, response time and

stability of the system. In addition, the current, control voltage, and electromagnetic torque signals are also recorded to analyze the characteristics of the motor when operating under the impact of speed changes.

Table 2. RBFNN parameters used in the experiment

Parameter	Value
n_j	5
η	0.5
$\boldsymbol{c}$	[-1 1]
b	1.2

Fig. 3 shows the motor speed response over time and the corresponding speed tracking error between the actual signal and the reference signal for two control methods: the conventional PID and the RBFNN controller. In Fig. 3 (a), both controllers track the reference signal quite well for most of the time. However, the RBFNN exhibits better tracking accuracy at many critical times, especially during fast transients such as the initial acceleration (t = 0–0.2 s), sudden speed changes ($t = 3.5s$ and $t = 7.5s$), and deceleration ($t = 7.5s - 10s$). The zoomed-in plots clearly show that the RBFNN significantly improves the tracking and reduces overshoot compared to the PID. Fig. 3 (b) clearly shows the difference in tracking error between the two methods. While both maintain small errors during steady-state periods, the PID controller struggles during periods of abrupt speed changes, typically at t = 6 s, when the error spikes and takes a long time to stabilize. In contrast, the RBFNN generates only a small error pulse and quickly returns to steady state, demonstrating superior adaptability to changing operating conditions.

Fig. 4 presents a detailed comparison of the current control performance between the PID and RBFNN controllers in both the synchronous rotating (a) and three-phase stator (b) reference frames. In the top left sub-plot, the direct shaft current i_d is expected to remain at or near zero under ideal field-oriented control to minimize core losses. Both controllers attempt to track this condition; however, the RBFNN exhibits higher ripple and noise in the i_d response than the PID controller. This may be due to the adaptive nature of the RBFNN in estimating model uncertainty. The lower-left subplot shows the quadrature-axis current i_q, which directly relates to the electromagnetic torque production. The RBFNN controller demonstrates superior tracking accuracy, especially during the dynamic load change around $t = 6s$, with faster convergence and smaller steady-state error than the PID. This indicates that the RBFNN more effectively compensates for nonlinearities and time-varying disturbances in the system.

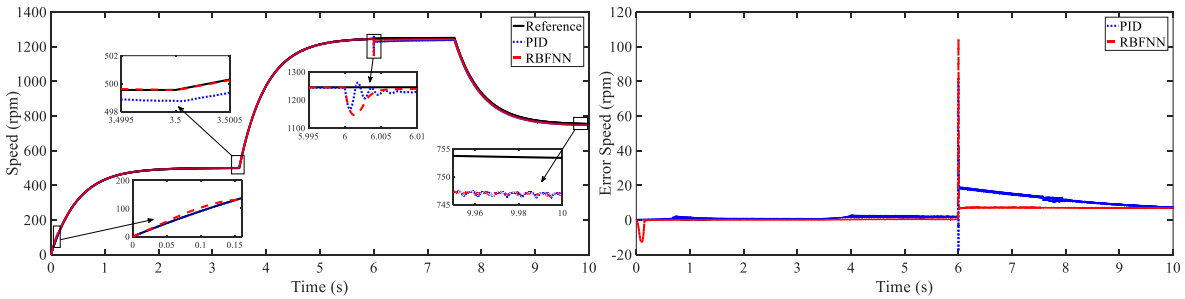

(a) Motor speed response (b) Speed tracking error

Fig. 3. Comparison of speed control performance between PID and RBFNN controllers

Fig. 4 (b) shows the three-phase stator current i_{abc} controlled by the RBFNN-based current controller. During the low-current steady-state period around $t = 1s$, the current amplitude is small and exhibits slight oscillations and phase shifts, which are attributed to the initial adaptive phase of the RBFNN. During the transient period near $t = 3.5s$, the current waveform shows increased high-

frequency components, indicating the presence of nonlinear adaptive compensation as the system responds to load changes. Despite this, the amplitude and symmetry of the waveform are still acceptable. It is worth noting that during high load steady-state operation at around $t = 6s$, the current achieves a clean sinusoid with appropriate phase separation, confirming that the RBFNN has fully adapted and stabilized the current injection process.

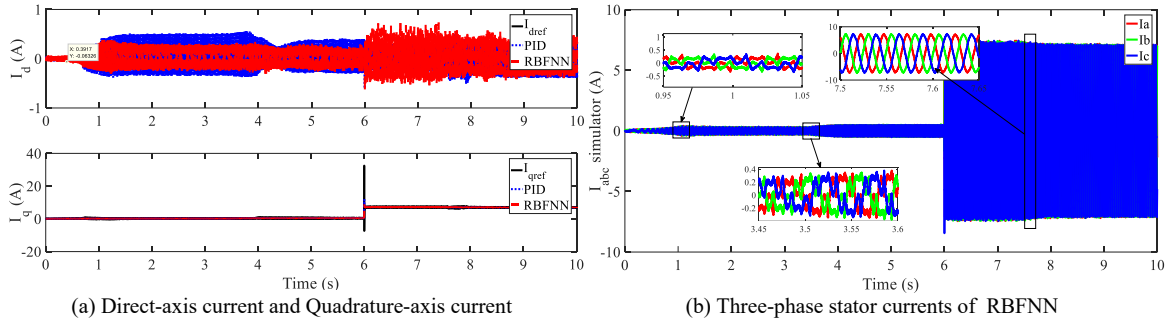

(a) Direct-axis current and Quadrature-axis current (b) Three-phase stator currents of RBFNN

Fig. 4. Current control performance using the RBFNN controller

4.2. Real-Time Implementation Results

In this case, the author used the Real-Time Digital Simulator Flagship OP5707XG system (shown Fig. 5) to simulate and control PMSM in real time, as in the previous section. This is a high-end real-time hardware device developed by OPAL-RT, equipped with a powerful 8-core Intel Xeon processor, integrated Xilinx Kintex-7 FPGA, and supporting flexible I/O connections, meeting the requirements in industrial control research and application. Thanks to its superior computing power and low latency, OP5707XG allows for the efficient implementation of the proposed control algorithms. Therefore, the author chose this tool to verify the stability of the proposed control method in a real-time environment, thereby creating a premise to get closer to practical applications.

Fig. 6 illustrates the speed tracking results of the PMSM motor in both simulation and real-time experiments. In Fig. 6 (a), it can be seen that the actual speeds achieved in both cases closely follow the reference signal over the three speed change stages. However, some small deviations still appear at the speed change times, in which the error in real-time experiments is more obvious due to the impact of noise and hardware delay. Fig. 6 (b) shows that the amplitude of the speed error in experiments is larger than that in simulation, especially noticeable at around 6 seconds. This reflects the difference between the ideal simulation environment and the actual operating conditions. However, the error is still within an acceptable limit, confirming that the proposed controller operates effectively in both simulation and real-time experiments.

Fig. 7 shows a comparison of the three-phase current i_{abc} of the PMSM motor in two cases: (a) real-time experiment on OPAL-RT hardware and (b) simulation in a virtual environment. In both cases, the current has a clear change through three stages corresponding to the load change. In the first stage $(0 - 3s)$, the current fluctuates with a small amplitude due to the inertia of the system which is accurately simulated in the device in real time. When entering the middle stage $(3s - 6.5s)$, the amplitude increases significantly, the current signal has a clearer sinusoidal shape, indicating that the system has reached a more stable operating mode. The last stage $(6.5s - 10s)$ is the stage of load existence appearing from $t = 6s$, the current increases sharply in amplitude in both cases; however the simulation has a more ideal waveform and less noise than the experiment. Notably, the zoomed-in images reveal the detailed difference: the simulated current signal is nearly ideal with a balanced three-phase sinusoidal waveform, while the experimental data is affected by real noise and hardware errors.

4.3. Comparison Results of Methods when Implementing Real-Time

In order to confirm the effectiveness of the proposed method, the author conducted a comparative study with typical controllers, including PID, FOPID, and FOPID optimized by the PSO algorithm.

The test scenarios were selected similarly to the previous sections, to ensure objectivity and transparency in the evaluation process. The comparison results will show apparent differences between the methods and highlight the superiority of the controller based on the proposed theory.

Fig. 5. Real-Time digital simulator flagship OP5707XG system

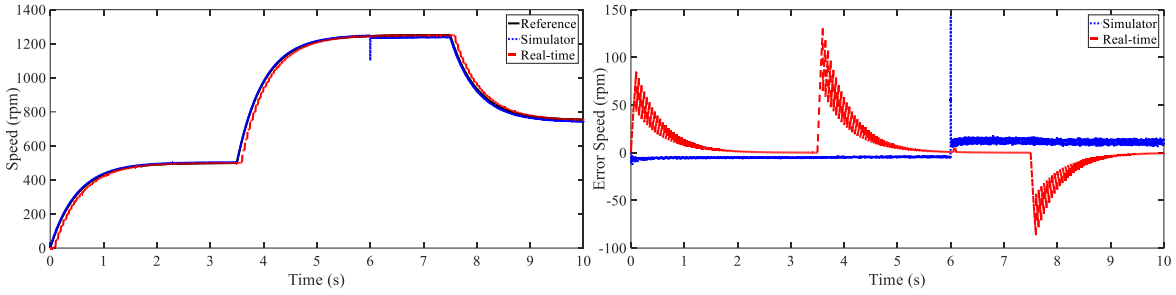

(a) Motor speed response (b) Speed tracking error

Fig. 6. Speed response and speed error of PMSM in both simulation and real-time experiments

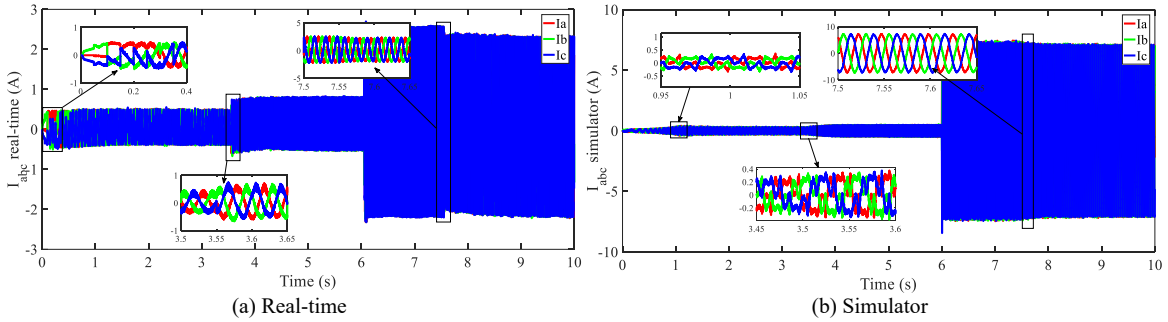

(a) Real-time (b) Simulator

Fig. 7. Comparison of three-phase stator current between real time and simulation

Observing Fig. 8 clearly shows the difference in the response of the controllers. The PID controller has a reasonably fast response speed, but oscillations and errors appear at some stages, as zoomed in the figure, especially when the system changes the desired value. FOPID helps improve the accuracy, but the stabilization speed is not optimal. When FOPID is optimized with PSO, the control quality is significantly improved: the error is reduced, the response is smoother than pure PID and FOPID, but there is still a small oscillation phenomenon in the transition region. Meanwhile, the RBFNN controller (red line) shows superior performance. The response curve closely follows the reference signal at most stages, the transition oscillation is small, and the steady-state error is almost

zero. In the zoomed regions, RBFNN demonstrates a clear advantage when it quickly converges to the desired value, limits oscillations, and maintains stability even when there is a sudden change in the desired value.

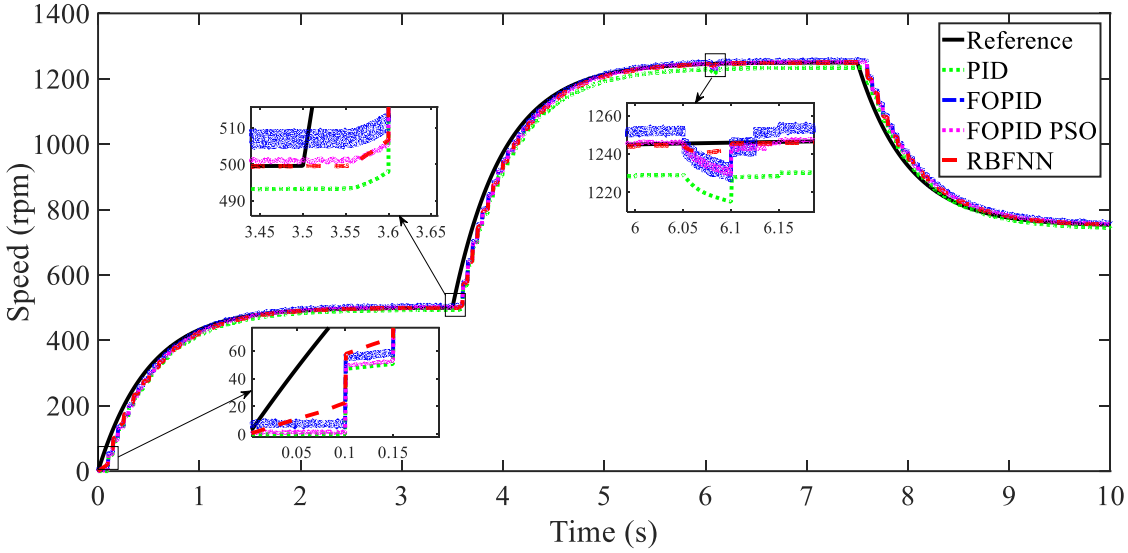

Fig. 8. Speed response and speed error of PMSM in both simulation and real-time experiments

Fig. 9 shows the system's speed error when using different controllers, including PID, FOPID, FOPID-PSO, and RBFNN. It can be observed that the PID controller (green line) maintains a larger error during the transient period and takes more time to converge to the desired value. FOPID (blue line) improves the error compared to PID, but still has significant oscillations when the system is subjected to disturbances or sudden changes. Optimizing FOPID with PSO (purple line) reduces oscillations and shortens the convergence time; however, the maximum error still appears clearly at the load change points. Meanwhile, the RBFNN controller (red line) performs better with significantly smaller maximum error amplitude, fast quenching time, and almost zero steady-state error. Especially when the system changes the reference value (about 3.5s and 7.5s), RBFNN gives the most stable response, quickly bringing the error back to near zero without causing prolonged oscillation. This demonstrates the RBF neural network's strong adaptive learning and generalization capabilities, helping the system maintain higher accuracy and stability than traditional control methods and algorithm-based optimization methods.

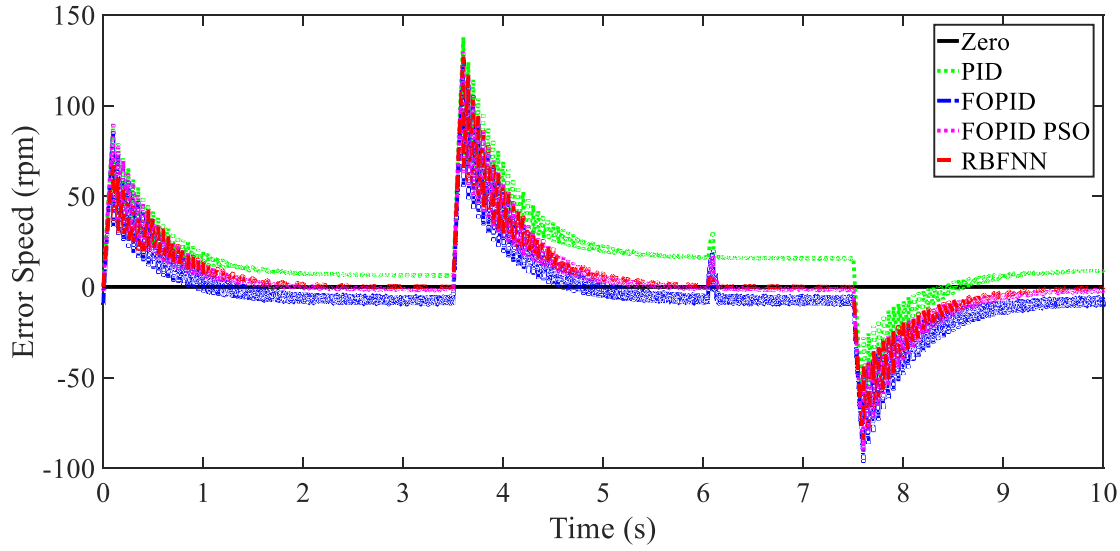

Fig. 9. Speed response and speed error of PMSM in both simulation and real-time experiments

The Fig. 10 shows a quantitative comparison of the errors of the PID, FOPID, FOPID-PSO, and RBFNN controllers according to the indices e_A, e_B, mse_A and mse_B. It can be clearly seen that the RBFNN consistently achieves the smallest error values in all four criteria, demonstrating its ability to reduce the overall error in both instantaneous and mean square values. In contrast, the PID and FOPID controllers have significantly higher errors, reflecting poor accuracy in tracking the output signal. The FOPID-PSO shows an improvement over the PID and FOPID, but still fails to achieve the low and stable error level of the RBFNN. This result is consistent with the speed response and error curves presented earlier: the RBFNN ensures fast and stable response and optimizes the error according to various criteria.

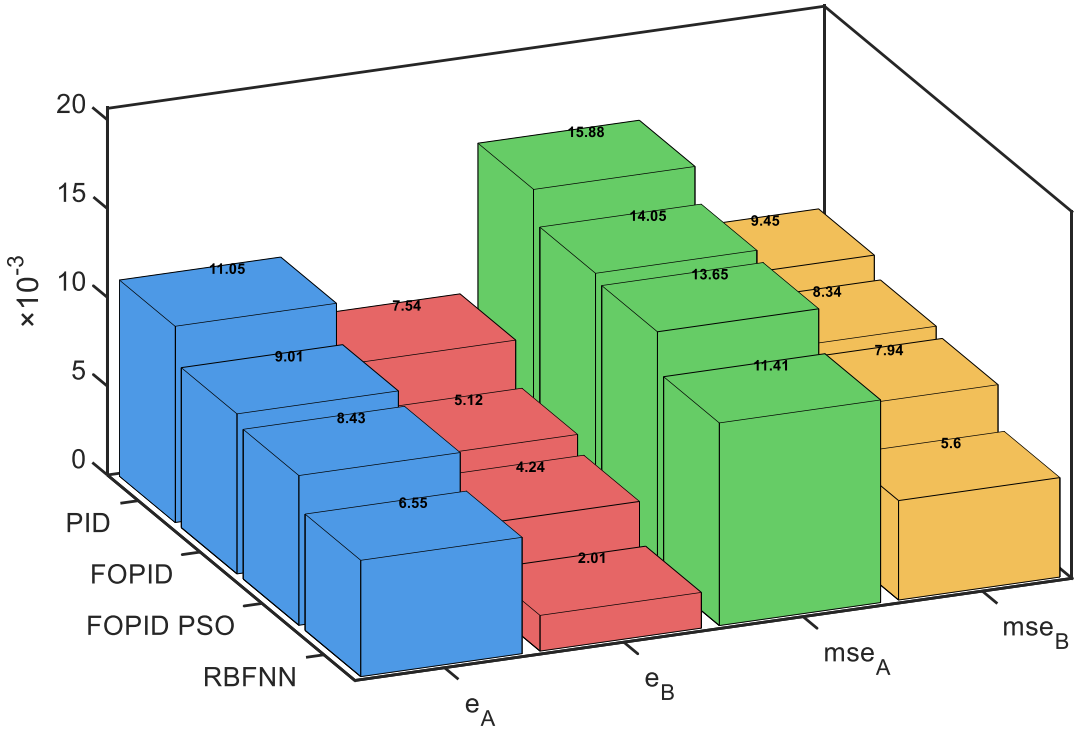

Fig. 10. Speed response and speed error of PMSM in both simulation and real-time experiments

5. Conclusion

This paper presents an advanced sliding mode control (SMC) scheme integrated with a Radial Basis Function Neural Network (RBFNN) to enhance the precision and robustness of speed regulation for permanent magnet synchronous motors (PMSMs). In the proposed method, the RBFNN is designed to directly estimate and compensate for unknown nonlinearities and external disturbances in real time, thereby effectively suppressing chattering and improving the disturbance rejection capability of the SMC. The closed-loop stability of the control system is rigorously guaranteed through Lyapunov theory, ensuring reliable operation under parameter variations and load disturbances.

To validate the feasibility and performance of the proposed approach, extensive simulations and real-time experiments were carried out on the OP5707XG hardware-in-the-loop platform. The comparative results against conventional PID, fractional-order PID (FOPID), and optimized FOPID-PSO controllers clearly demonstrate that the RBFNN–SMC achieves faster transient response, reduced overshoot, smaller steady-state error, and superior robustness against sudden load changes. In particular, the error response curves indicate that the proposed controller maintains minimal error with rapid convergence, outperforming benchmark methods in dynamic and steady-state conditions.

The results confirm that the proposed RBFNN–SMC ensures accurate and reliable PMSM speed regulation and provides a flexible framework that can be extended to current control and generalized to other motor drive systems. The novelty and significance of this work lie in the effective combination

of neural network learning capability with sliding mode robustness, offering a promising solution for high-performance drive applications requiring precision, adaptability, and resilience to disturbances.

Author Contribution: All authors contributed equally to the main contributor to this paper. All authors read and approved the final paper.

Acknowledgment: The author would like to sincerely thank the Faculty of Automotive Engineering Technology, Ho Chi Minh City University of Industry, for investing and supporting the Real-Time Digital Simulator Flagship OP5707XG equipment and the facilities that helped the author carry out this research.

Conflicts of Interest: The authors declare no conflict of interest.

References

[1] F. Chen, J. Fan, W. Li, J. Fang, S. Ding, "Mitigation of high-resistance connection in surface-mounted PMSM drive system based on model predictive current control," *Results in Engineering*, vol. 15, p. 100590, 2022, https://doi.org/10.1016/j.rineng.2022.100590.

[2] S. Gao, Y. Wei, D. Zhang, H. Qi, Y. Wei and Z. Yang, "Model-Free Hybrid Parallel Predictive Speed Control Based On Ultralocal Model of PMSM for Electric Vehicles," *IEEE Transactions on Industrial Electronics*, vol. 69, no. 10, pp. 9739-9748, 2022, https://doi.org/10.1109/TIE.2022.3159951.

[3] R. Yan, D. Wang, C. Wang, W. Miao and X. Wang, "Analytical Approach and Experimental Validation of Sideband Electromagnetic Vibration and Noise in PMSM Drive With Voltage-Source Inverter by SVPWM Technique," *IEEE Transactions on Magnetics*, vol. 61, no. 1, pp. 1-6, 2025, https://doi.org/10.1109/TMAG.2024.3498051.

[4] H. Cao *et al*., "Improved Deadbeat Predictive Current Control of PMSM Drives With Repetitive Control-Based Disturbance Correction Observer," *IEEE Transactions on Power Electronics*, vol. 40, no. 1, pp. 801-812, 2025, https://doi.org/10.1109/TPEL.2024.3482315.

[5] T. Yazdan, M. Humza and H. -W. Cho, "Three-Phase Dual-Winding Multitasked PMSM Machine Using Double Layer Concentrated Winding for HEV Application," *IEEE Access*, vol. 11, pp. 36682-36691, 2023, https://doi.org/10.1109/ACCESS.2023.3264568.

[6] S. Thangavel, D. Mohanraj, T. Girijaprasanna, S. Raju, C. Dhanamjayulu and S. M. Muyeen, "A Comprehensive Review on Electric Vehicle: Battery Management System, Charging Station, Traction Motors," *IEEE Access*, vol. 11, pp. 20994-21019, 2023, https://doi.org/10.1109/ACCESS.2023.3250221.

[7] M. R. Khowja, K. Singh, A. la Rocca, G. Vakil, R. Ramnathan and C. Gerada, "Fault-Tolerant Dual Channels Three-Phase PMSM for Aerospace Applications," *IEEE Access*, vol. 12, pp. 126845-126857, 2024, https://doi.org/10.1109/ACCESS.2024.3451705.

[8] W. Deng, X. Zhang and B. Yan, "An Enhanced Discrete Virtual Vector-Based Direct Torque Control of PMSM Drives," *IEEE Transactions on Energy Conversion*, vol. 39, no. 1, pp. 277-286, 2024, https://doi.org/10.1109/TEC.2023.3314521.

[9] H. Zhou, C. Chen, X. Xiang and G. Liu, "Switching-Table-Based Diagnosis-Free Fault-Tolerant DTC for Five-Phase PMSM With Any Phase Open-Circuit Fault," *IEEE Transactions on Industrial Electronics*, vol. 71, no. 11, pp. 13790-13800, 2024, https://doi.org/10.1109/TIE.2024.3379662.

[10] Basil and H. M. Marhoon, "Correction to: selection and evaluation of FOPID criteria for the X-15 adaptive flight control system (AFCS) via Lyapunov candidates: Optimizing trade-offs and critical values using optimization algorithms," *e-Prime - Advances in Electrical Engineering, Electronics and Energy*, vol. 8, p. 100589, 2024, https://doi.org/10.1016/j.prime.2024.100589.

[11] A. A. Al-Jazaeri, M. Z. Al-Faiz, "The Optimum Design of Interval Type-2 Fuzzy Controller for 5 DOF Robotic Manipulator," *Iraqi Journal of Information and Communications Technology*, vol. 1, no. 1, pp. 36-51, 2018, https://doi.org/10.31987/ijict.1.1.10.

[12] N. Basil, H. M. Marhoon, D. F. Sahib, A. F. Mohammed, H. M. Ridha & A. Ma'arif, "Accelerated black hole optimization algorithm with enhanced FOPID controller for omni-wheel drive mobile robot system,"

Neural Computing and Applications, vol. 37, pp. 16983-17014, 2025, https://doi.org/10.1007/s00521-025-11310-6.

[13] T.-H. Liu, Y.-H. Zhuang, "Maximum efficiency control and predictive-speed controller design for interior permanent magnet synchronous motor drive systems," *Frontiers in Electronics*, vol. 3, pp. 1-13, 2022, https://doi.org/10.3389/felec.2022.904976.

[14] J. Feng, "Parameter fuzzy rectification for sliding mode control of five-phase permanent magnet synchronous motor speed control system," *Frontiers in Mechanical Engineering*, vol. 10, 2024, https://doi.org/10.3389/fmech.2024.1391593.

[15] Z. Liu, X. Huang, Q. Hu, G. Yang, Y. Wang and J. Shen, "Model-Free Predictive Current Control of PMSM Using Modified Extended State Observer," *IEEE Transactions on Power Electronics*, vol. 40, no. 1, pp. 679-690, 2025, https://doi.org/10.1109/TPEL.2024.3476318.

[16] J. Mao *et al*., "Non-Cascaded Model-Free Predictive Speed Control of SMPMSM Drive System," *IEEE Transactions on Energy Conversion*, vol. 37, no. 1, pp. 153-162, 2022, https://doi.org/10.1109/TEC.2021.3090427.

[17] K. Zhao, X. Chen, J. Liu and J. Yu, "Discrete-Time Adaptive Fuzzy Event-Triggered Control for PMSMs With Voltage Faults via Command Filter Approximator," *IEEE Transactions on Power Electronics*, vol. 39, no. 6, pp. 7343-7350, 2024, https://doi.org/10.1109/TPEL.2024.3369055.

[18] I. A. Hasan and O. A. Awad, "An optimized fuzzy logic controller for wireless network control system using PSO," *Iraqi Journal of Information and Communication Technology*, vol. 5, no. 1, pp. 1-15, 2022, https://doi.org/10.31987/ijict.5.1.180.

[19] H. S. Abdulkareem and O. A. Awad, "Fuzzy Set-Point Weight for PID Controller Based on Antlion Optimizer to Congestion Avoidance in TCP/AQM Routers," *Iraqi Journal of Information and Communication Technology*, vol. 2, no. 4, pp. 1-10, 2019, https://doi.org/10.31987/ijict.2.4.73.

[20] Q. Hou, Y. Zuo, J. Sun, C. H. T. Lee, Y. Wang and S. Ding, "Modified Nonlinear Active Disturbance Rejection Control for PMSM Speed Regulation With Frequency Domain Analysis," *IEEE Transactions on Power Electronics*, vol. 38, no. 7, pp. 8126-8134, 2023, https://doi.org/10.1109/TPEL.2023.3262519.

[21] Z. Hao *et al*., "Linear/Nonlinear Active Disturbance Rejection Switching Control for Permanent Magnet Synchronous Motors," *IEEE Transactions on Power Electronics*, vol. 36, no. 8, pp. 9334-9347, 2021, https://doi.org/10.1109/TPEL.2021.3055143.

[22] V. Djordjevic, H. Tao, X. Song, S. He, W. Gao, V. Stojanovic, "Data-driven control of hydraulic servo actuator: an event-triggered adaptive dynamic programming approach," *Mathematical Biosciences an Engineering*, vol. 20, no. 5, pp. 8561-8582, 2022, https://doi.org/10.3934/mbe.2023376.

[23] J. Zhao, "Data-Driven Adaptive Dynamic Programming for Optimal Control of Continuous-Time Multicontroller Systems With Unknown Dynamics," *IEEE Access*, vol. 10, pp. 41503-41511, 2022, https://doi.org/10.1109/ACCESS.2022.3168032.

[24] T. Sun, L. Cheng, W. Wang, and Y. Pan, "Semiglobal exponential control of Euler–Lagrange systems using a sliding-mode disturbance observer," *Automatica*, vol. 112, p. 108677, 2020, https://doi.org/10.1016/j.automatica.2019.108677.

[25] M. Chen, G. Tao and B. Jiang, "Dynamic Surface Control Using Neural Networks for a Class of Uncertain Nonlinear Systems With Input Saturation," *IEEE Transactions on Neural Networks and Learning Systems*, vol. 26, no. 9, pp. 2086-2097, 2015, https://doi.org/10.1109/TNNLS.2014.2360933.

[26] T. Yang, N. Sun and Y. Fang, "Adaptive Fuzzy Control for Uncertain Mechatronic Systems With State Estimation and Input Nonlinearities," *IEEE Transactions on Industrial Informatics*, vol. 18, no. 3, pp. 1770-1780, 2022, https://doi.org/10.1109/TII.2021.3089143.

[27] S. Roy, S. Baldi, and L. Fridman, "On adaptive sliding mode control without a priori bounded uncertainty," *Automatica*, vol. 111, p. 108650, 2020, https://doi.org/10.1016/j.automatica.2019.108650.

[28] Q. Deng, Y. Peng, T. Han and D. Qu, "Event-Triggered Bipartite Consensus in Networked Euler–Lagrange Systems With External Disturbance," *IEEE Transactions on Circuits and Systems II: Express Briefs*, vol. 68, no. 8, pp. 2870-2874, 2021, https://doi.org/10.1109/TCSII.2021.3057859.

[29] J. Han, "From PID to Active Disturbance Rejection Control," *IEEE Transactions on Industrial Electronics*, vol. 56, no. 3, pp. 900-906, 2009, https://doi.org/10.1109/TIE.2008.2011621.

[30] W. -H. Chen, J. Yang, L. Guo and S. Li, "Disturbance-Observer-Based Control and Related Methods—An Overview," *IEEE Transactions on Industrial Electronics*, vol. 63, no. 2, pp. 1083-1095, 2016, https://doi.org/10.1109/TIE.2015.2478397.

[31] W. He, Y. Sun, Z. Yan, C. Yang, Z. Li and O. Kaynak, "Disturbance Observer-Based Neural Network Control of Cooperative Multiple Manipulators With Input Saturation," *IEEE Transactions on Neural Networks and Learning Systems*, vol. 31, no. 5, pp. 1735-1746, 2020, https://doi.org/10.1109/TNNLS.2019.2923241.

[32] M. Basin and P. Ramirez, "Sliding mode controller design for linear systems with unmeasured states," *Journal of the Franklin Institute*, vol. 349, no. 4, pp. 1337-1349, 2012, https://doi.org/10.1016/j.jfranklin.2011.06.019.

[33] H. Wu and P. Shi, "Adaptive variable structure state estimation for uncertain systems with persistently bounded disturbances," *International Journal of Robust and Nonlinear Control*, vol. 20, no. 17, pp. 2003-2015, 2010, https://doi.org/10.1002/rnc.1567.

[34] L. Wu, P. Shi and H. Gao, "State Estimation and Sliding-Mode Control of Markovian Jump Singular Systems," *IEEE Transactions on Automatic Control*, vol. 55, no. 5, pp. 1213-1219, 2010, https://doi.org/10.1109/TAC.2010.2042234.

[35] Y. Xia, H. Yang, M. Fu, and P. Shi, "Sliding mode control for linear systems with time-varying input and state delays," *Circuits, Systems, and Signal Processing*, vol. 30, no. 3, pp. 629-641, 2011, https://doi.org/10.1007/s00034-010-9237-x.

[36] İ. Eker, "Second-order sliding mode control with experimental application," *ISA Transactions*, vol. 49, no. 3, pp. 394-405, 2010, https://doi.org/10.1016/j.isatra.2010.03.010.

[37] H. F. Ho, Y. K. Wong, and A. B. Rad, "Adaptive fuzzy sliding mode control with chattering elimination for nonlinear SISO systems," *Simulation Modelling Practice and Theory*, vol. 17, no. 7, pp. 1199-1210, 2009, https://doi.org/10.1016/j.simpat.2009.04.004.

[38] J. Hu, Z. Wang, H. Gao, and L. K. Stergioulas, "Robust H∞ sliding mode control for discrete time-delay systems with stochastic nonlinearities," *Journal of the Franklin Institute*, vol. 349, no. 4, pp. 1459-1479, 2012, https://doi.org/10.1016/j.jfranklin.2011.05.018.

[39] T. Sun, H. Pei, Y. Pan, H. Zhou, and C. Zhang, "Neural network-based sliding mode adaptive control for robot manipulators," *Neurocomputing*, vol. 74, no. 14, pp. 2377-2384, 2011, https://doi.org/10.1016/j.neucom.2011.03.015.

[40] M. S. Kahkeshi, F. Sheikholeslam, and M. Zekri, "Design of adaptive fuzzy wavelet neural sliding mode controller for uncertain nonlinear systems," *ISA Transactions*, vol. 52, no. 3, pp. 342-350, 2013, https://doi.org/10.1016/j.isatra.2013.01.004.

[41] L. Zhang, Z. Chen, X. Yu, J. Yang and S. Li, "Sliding-Mode-Based Robust Output Regulation and Its Application in PMSM Servo Systems," *IEEE Transactions on Industrial Electronics*, vol. 70, no. 2, pp. 1852-1860, 2023, https://doi.org/10.1109/TIE.2022.3163536.

[42] X. Miao, W. Yao, H. Ouyang, Z. Zhu, "Novel composite speed control of permanent magnet synchronous motor using integral sliding mode approach," *Mathematics*, vol. 11, no. 22, p. 4666, 2023, https://doi.org/10.3390/math11224666.

[43] S. Kuppusamy and Y. H. Joo, "Memory-Based Integral Sliding-Mode Control for T–S Fuzzy Systems With PMSM via Disturbance Observer," *IEEE Transactions on Cybernetics*, vol. 51, no. 5, pp. 2457-2465, 2021, https://doi.org/10.1109/TCYB.2019.2953567.

[44] C. Zhang, R. Qi, B. Li, S. Riaz, "Experimental validation and analysis of hybrid adaptive iterative learning sliding mode control for PMSM seeker coordinator," *Engineering Science and Technology, an International Journal*, vol. 58, p. 101826, 2024, https://doi.org/10.1016/j.jestch.2024.101826.

[45] S. H. Hosseini, M. Tabatabaei, "IPMSM velocity and current control using MTPA based adaptive fractional order sliding mode controller," *Engineering Science and Technology, an International Journal*, vol. 20, no. 3, pp. 896-908, 2017, https://doi.org/10.1016/j.jestch.2017.03.008.

[46] P. Chen and Y. Luo, "Analytical Fractional-Order PID Controller Design With Bode's Ideal Cutoff Filter for PMSM Speed Servo System," *IEEE Transactions on Industrial Electronics*, vol. 70, no. 2, pp. 1783-1793, 2023, https://doi.org/10.1109/TIE.2022.3158009.

[47] L. Zhang, H. Li, L. Shan, L. Zhang, L. Zhang, "Double-hierarchical fuzzy exponential convergence law fractional-order sliding mode montrol for PMSM drive control in EV," *Engineering Science and Technology, an International Journal*, vol. 47, p. 101536, 2023, https://doi.org/10.1016/j.jestch.2023.101536.

[48] D. Nicolis, F. Allevi and P. Rocco, "Operational Space Model Predictive Sliding Mode Control for Redundant Manipulators," *IEEE Transactions on Robotics*, vol. 36, no. 4, pp. 1348-1355, 2020, https://doi.org/10.1109/TRO.2020.2974092.

[49] L. Wu, J. Liu, S. Vazquez and S. K. Mazumder, "Sliding Mode Control in Power Converters and Drives: A Review," *IEEE/CAA Journal of Automatica Sinica*, vol. 9, no. 3, pp. 392-406, 2022, https://doi.org/10.1109/JAS.2021.1004380.

[50] S. Wang, J. Na and Q. Chen, "Adaptive Predefined Performance Sliding Mode Control of Motor Driving Systems With Disturbances," *IEEE Transactions on Energy Conversion*, vol. 36, no. 3, pp. 1931-1939, 2021, https://doi.org/10.1109/TEC.2020.3038010.

[51] J. Qiu, W. Ji and M. Chadli, "A Novel Fuzzy Output Feedback Dynamic Sliding Mode Controller Design for Two-Dimensional Nonlinear Systems," *IEEE Transactions on Fuzzy Systems*, vol. 29, no. 10, pp. 2869-2877, 2021, https://doi.org/10.1109/TFUZZ.2020.3008271.

[52] T. Orlowska-Kowalska *et al*., "Fault Diagnosis and Fault-Tolerant Control of PMSM Drives–State of the Art and Future Challenges," *IEEE Access*, vol. 10, pp. 59979-60024, 2022, https://doi.org/10.1109/ACCESS.2022.3180153.

[53] A. Najem, A. Moutabir, A. Ouchatti, M. Haissouf, "Experimental Validation of the Generation of Direct and Quadratic Reference Currents by Combining the Ant Colony Optimization Algorithm and Sliding Mode Control in PMSM using the Process PIL," *International Journal of Robotics and Control Systems*, vol. 4, no. 1, pp. 188-216, 2024, https://doi.org/10.31763/ijrcs.v4i1.1286.

[54] L. Wang, J. Mishra, Y. Zhu and X. Yu, "An Improved Sliding-Mode Current Control of Induction Machine in Presence of Voltage Constraints," *IEEE Transactions on Industrial Informatics*, vol. 16, no. 2, pp. 1182-1191, 2020, https://doi.org/10.1109/TII.2019.2944228.

[55] Z. Wang, Y. Z. Zhu, H. Xue, and H. J. Liang, "Neural networks-based adaptive event-triggered consensus control for a class of multi-agent systems with communication faults," *Neurocomputing*, vol. 470, pp. 99-108, 2022, https://doi.org/10.1016/j.neucom.2021.10.059.

[56] X. Zhao, P. Shi, X. Zheng and J. Zhang, "Intelligent Tracking Control for a Class of Uncertain High-Order Nonlinear Systems," *IEEE Transactions on Neural Networks and Learning Systems*, vol. 27, no. 9, pp. 1976-1982, 2016, https://doi.org/10.1109/TNNLS.2015.2460236.

[57] W. He, Y. Dong and C. Sun, "Adaptive Neural Impedance Control of a Robotic Manipulator With Input Saturation," *IEEE Transactions on Systems, Man, and Cybernetics: Systems*, vol. 46, no. 3, pp. 334-344, 2016, https://doi.org/10.1109/TSMC.2015.2429555.

[58] T. Q. Ngo, M. K. Duong, D. C. Pham, and D. -N. Nguyen, "Adaptive Wavelet CMAC Tracking Control for Induction Servomotor Drive System," *Journal of Electrical Engineering & Technology*, vol. 14, no. 1, pp. 209-218, 2019, https://doi.org/10.1007/s42835-018-00029-1.

[59] R. Yang, C. Yang, M. Chen, and A. S. Annamalai, "Discrete-time optimal adaptive RBFNN control for robot manipulators with uncertain dynamics," *Neurocomputing*, vol. 234, pp. 107-115, 2017, https://doi.org/10.1016/j.neucom.2016.12.048.

[60] Z. Wang, J. Yuan, Y. Pan, and J. Wei, "Neural network-based adaptive fault tolerant consensus control for a class of high order multi-agent systems with input quantization and time-varying parameters," *Neurocomputing*, vol. 266, pp. 315-324, 2017, https://doi.org/10.1016/j.neucom.2017.05.043.

[61] T. H. Tran, T. Q. Ngo, H. T. T. Uyen, V. T. Nguyen, and T. Đoan Duong, "Adaptive Task-Space Control of Five-Bar Parallel Robot Dynamic Model with Fully Unknown Using Radial Basis Function Neural

Networks for High-Precision Applications," *Journal of Robotics and Control (JRC)*, vol. 6, no. 4, pp. 1624-1635, 2025, https://doi.org/10.18196/jrc.v6i4.26537.

[62] M. Daachi, T. Madani, B. Daachi, and K. Djouani, "A radial basis function neural network adaptive controller to drive a powered lower limb knee joint orthosis," *Applied Soft Computing*, vol. 34, pp. 324-336, 2015, https://doi.org/10.1016/j.asoc.2015.04.034.

[63] H. R. Nohooji, "Constrained neural adaptive PID control for robot manipulators," *Journal of the Franklin Institute*, vol. 357, no. 7, pp. 3907-3923, 2020, https://doi.org/10.1016/j.jfranklin.2019.12.042.

[64] S. Seshagiri and H. K. Khalil, "Output feedback control of nonlinear systems using RBF neural networks," *IEEE Transactions on Neural Networks*, vol. 11, no. 1, pp. 69-79, 2000, https://doi.org/10.1109/72.822511.

[65] P. Pillay and R. Krishnan, "Modeling of permanent magnet motor drives," *IEEE Transactions on Industrial Electronics*, vol. 35, no. 4, pp. 537-541, 1988, https://doi.org/10.1109/41.9176.

[66] F. Mohd Zaihidee, S. Mekhilef, and M. Mubin, "Robust speed control of PMSM using sliding mode control (SMC)—A review," *Energies*, vol. 12, no. 9, p. 1669, 2019, https://doi.org/10.3390/en12091669.